Open Access
Full Length Article

ORIGINAL ARTICLE

Implementation of Periodic Boundary Conditions in FDTD Algorithm

Abdul Aleem Jamali[1], M. Rizwan Amirzada[2], M. R. Anjum[3], Kelash Kanwar[4]

[1,4] Department of Electronic Engineering, Quaid-e-Awam University of Engineering, Science and Technology, Nawabshah
[2] Faculty of Engineering and Computer Science, National University of Modern Languages, Islamabad
[3] Department of Electronic Engineering, The Islamia University Bahawalpur, Pakistan

ABSTRACT

This paper presents the implementation of Periodic Boundary Conditions in Finite Difference Time Domain (FDTD) algorithm for the computation of periodic structures. Many electromagnetic problems such as in photonic crystals, scattering and radiation, the periodic scatterers are used. The periodicity of the scatterers is employed to simplify electromagnetic analysis by considering it for an infinite-array. Among other numerical techniques, FDTD provides efficient performance when the number of unknown (or problem size) increases together with covering wide band of frequencies in single simulation. An extensive number of simulated experiments are performed to demonstrate the efficient implementation of PBCs by using FDTD algorithm.

Keywords: Finite difference time domain (FDTD) method, Periodic structures, Periodic boundary condition (PBC), Absorbing boundary condition, Computational electromagnetic.

Author`s Contribution
[1,2,3]Manuscript writing, Data analysis, interpretation, Conception, synthesis, planning of research, Interpretation and discussion, Data Collection

Address of Correspondence
Abdul Aleem Jamali
Email: jamali.abdulaleem@quest.edu.pk

Article info.
Received: July 16, 2017
Accepted: Oct 13, 2018
Published: Dec 30, 2018

Cite this article: *Jamali AA, Amirzada MR, Anjum MR, Kanwar K. Implementation of Periodic Boundary Conditions in FDTD Algorithm. J. Inf. commun. technol. robot. appl.2018; 9(2):28-36.*

Funding Source: *Nil*
Conflict of Interest: *Nil*

INTRODUCTION

With the advancement of computer technology and rapid increase of computational resources, computational electromagnetic (CEM) is widely used by engineers and researchers. CEM is used to calculate the electromagnetic response of antennas, wave guiding, radiation and scattering phenomena, microwave and optical devices[1, 2]. The FDTD method is easy to formulate in comparison to different numerical techniques[3]. It is used in computer simulation models without complexity and provides suitable and unique solution for electromagnetic analysis of structures[2]. It can easily model various media including dielectrics, conductors, magnetic, lumped-elements, frequency-dependent, nonlinear, and anisotropic[4-6]. FDTD method is an attractive technique to solve broad range of microwave and optical problems[7-10]. These advantages of FDTD have made it to be used widely in many electromagnetic (EM) applications. Those applications comprise of the conventional EM problems, such as scattering and radar cross section (RCS) calculations, designs of microwave circuits, waveguides and fiber optics, and pattern characterizations of antenna[11-14]. The FDTD method also

has a strong capability to solve the scenarios, such as interaction of wave with human bodies and electromagnetic interference (EMI) in high speed electronics[9,13]. Periodic structures have been greatly found in the nature, which have captured the interest of both the artists and scientists. When electromagnetic waves interact with the periodic structures, an interesting phenomenon occurs[6,12,15]. Many electromagnetic problems such as in scattering and radiation, the periodic scatterers are present. The periodicity of the scatterers is used to simplify the problem by considering it for an infinite-array[16]. This analysis can also be done by using FDTD method, by taking the periodicity for an infinite-array in one or two dimensions. In conventional EM problems such as in scattering and radiation, the fields propagate to infinity. The representation of the real electromagnetic assumption, computational domain must be theoretically extended to infinity[14]. Nevertheless, the computational domain should be reduced to a finite size because of the computational machines memory limitation[17-21]. This can be implemented by using proper boundary condition at the boundary of the computational domain for infinite extension of the simulation and for eliminating reflected wave. Different absorbing boundary conditions have been developed for providing reflection free truncation[17]. One of these techniques is the Convolutional Perfectly Matched Layer (CPML), which has a lot of advantages such as it is highly absorptive for evanescent waves and provides significant memory saving[22-26]. Periodic boundary conditions (PBCs) are implemented for the computation of infinite structure with one or two dimensional periodicity[15]. For example, Frequency Selective Surfaces (FSS), photonic bandgap, corrugated waveguides, and double negative materials have periodic structures[5,11,13]. An intimate antenna array is also considered as a periodic structure. Different techniques have been proposed for using PBCs. These can be classified into Direct Field Methods and Field Transformation Methods[9]. Field Transformation Methods use field transformation technique to eliminate the need of time advanced data, while, Direct Field Methods use directly Maxwell's equations with PBCs. Floquet theory which is based on latter method is the foundation for developing PBCs[5,11,15,17].

In this paper, the PBC is implemented by using FDTD method. Section 1, provides the brief introduction of PBCs with its applications. Section 2 describes the FDTD method in detail, starting with Yee's cell1 and updating scheme for PBCs. Section 3 provides implementation of boundary conditions for two-dimensional computational domain. Section 4 demonstrates results and discusses those results. Finally section 5 concludes the demonstrated research work.

RESEARCH METHODOLOGY

The PBCs are implemented by using FDTD algorithm. The Yee's discretization technique is used to discretize differential form of Maxwell's equations[1]. In the following sub-section, the Yee's technique is discussed in detail for the computation and updating of the electric and magnetic field components of Maxwell's equations.

Yee's cell and updating scheme

In general, there are four Maxwell's equations, among these equations only two equations are required for the implementation of FDTD method. The differential form of the two Maxwell's equations[27], required for FDTD algorithm is given as,

$$\nabla \times \underline{\boldsymbol{E}}(\underline{\boldsymbol{R}},t) = -\frac{\partial}{\partial t}\underline{\boldsymbol{B}}(\underline{\boldsymbol{R}},t) - \underline{\boldsymbol{J}}_{\boldsymbol{m}}(\underline{\boldsymbol{R}},t), \quad (1)$$

$$\nabla \times \underline{\boldsymbol{H}}(\underline{\boldsymbol{R}},t) = \frac{\partial}{\partial t}\underline{\boldsymbol{D}}(\underline{\boldsymbol{R}},t) + \underline{\boldsymbol{J}}_{\boldsymbol{e}}(\underline{\boldsymbol{R}},t). \quad (2)$$

Constitutive relations are used to supplement Maxwell's equations and provide the material properties[11]. Constitutive equations for vacuum are:

$$\underline{\boldsymbol{D}}(\underline{\boldsymbol{R}},t) = \epsilon_0 \underline{\boldsymbol{E}}(\underline{\boldsymbol{R}},t),$$
$$\underline{\boldsymbol{B}}(\underline{\boldsymbol{R}},t) = \mu_0 \underline{\boldsymbol{H}}(\underline{\boldsymbol{R}},t),$$
$$\underline{\boldsymbol{J}}_{\boldsymbol{e}}{}^{con}(\underline{\boldsymbol{R}},t) = \sigma_e \underline{\boldsymbol{E}}(\underline{\boldsymbol{R}},t).$$

The $\underline{\boldsymbol{E}}(\underline{\boldsymbol{R}},\boldsymbol{t})$ and $\underline{\boldsymbol{H}}(\underline{\boldsymbol{R}},\boldsymbol{t})$ are the three-dimensional space vectors, so equations (eq. (1) and eq. (2)) represents three equations of each. These six equations are discretized in space and time by using finite difference scheme. Yee[1] has introduced a cubic lattice for the discretization of the computational space to solve differential form of Maxwell's equations. For the spatial-domain, magnetic (***H***) fields are discretized in middle of the cubic faces whereas electric (***E***) fields are sampled at the center of the edges[8]. By this way, each $\underline{\boldsymbol{E}}$ component is encircled by $\underline{\boldsymbol{H}}$ components, and each $\underline{\boldsymbol{H}}$ component is encircled by $\underline{\boldsymbol{E}}$ components. In the time-domain, electric and magnetic field components are computed at a half time step difference, such as magnetic field is sampled at

$t=(n_t+1)\Delta t$[11]. Whereas, the electric field is sampled at $t=(nt+1/2)\Delta t$[11]. For a two-dimensional simulation, transverse magnetic (TM) mode or transverse electric (TE) mode can be selected[8]. TM_y mode is selected in this work; which is composed of E_y, H_x, H_z components, as shown in Figure 1.

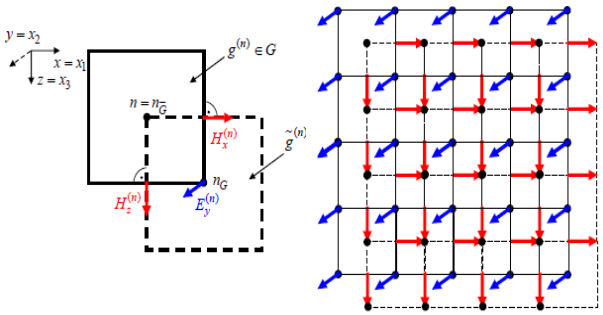

Figure 1: Two-dimensional staggered grid system in the 2-D TM case[8,9]. Red arrows show magnetic components, while white arrows show electric field components. Magnetic field components are along horizontal and vertical direction of the page, electric field components are normal to the page.

Then, the updating equations for the 2-D TM_y case leading to[8,20],

$$H_x^{(n_x,\,n_z,\,n_t)} = H_x^{(n_x,\,n_z,\,n_t-1)} + \frac{\Delta t}{\mu_0}\left[\frac{E_y^{(n_x,\,n_z+1/2,\,n_t-1/2)} - E_y^{(n_x,\,n_z-1/2,\,n_t-1/2)}}{\Delta z}\right], \quad (3)$$

$$H_z^{(n_x,\,n_z,\,n_t)} = H_z^{(n_x,\,n_z,\,n_t-1)} - \frac{\Delta t}{\mu_0}\left[\frac{E_y^{(n_x+1/2,\,n_z,\,n_t-1/2)} - E_y^{(n_x-1/2,\,n_z,\,n_t-1/2)}}{\Delta x}\right], \quad (4)$$

$$E_y^{(n_x+1/2,\,n_z+1/2,\,n_t+1/2)} = E_y^{(n_x+1/2,\,n_z+1/2,\,n_t-1/2)} - \frac{\Delta t}{\epsilon_0}\left[\frac{H_x^{(n_x,\,n_z+1,\,n_t)} - H_x^{(n_x,\,n_z,\,n_t)}}{\Delta z} - \frac{H_z^{(n_x+1,\,n_z,\,n_t)} - H_z^{(n_x,\,n_z,\,n_t)}}{\Delta x}\right]. \quad (5)$$

This time-stepping procedure is fully explicit; hence does not require any matrix inversion. This is the one of the advantages of FDTD method which makes it easy to implement[4-6,18]. To avoid instability (numerical) in FDTD method, time step size Δt must be smaller than the specific limit which is determined by the lattice space increments Δx, Δy, and Δz. In FD method, a minimum time of $\Delta t = \Delta x/c_0$ is required to propagate at a distance of one cell[9,20]. In a two-dimensional simulation, the propagation is allowed in the diagonal direction, hence the minimum time of $\Delta t = \Delta x/\sqrt{2}\,c_0$ is required. In general, the Courant condition is given as $\Delta t = \Delta x/\sqrt{(n.c)}$, where c and n are the speed of light in vacuum and the dimension of simulation, respectively[8].

Boundary conditions

Boundary condition for homogeneous case is given as[12]

$$\underline{\boldsymbol{E}}_{tan}(\underline{\boldsymbol{R}}, t) = \underline{\mathbf{0}}, \quad (6)$$

$$B_{normal}(\underline{\boldsymbol{R}}, t) = 0. \quad (7)$$

In order to solve partial differential equations numerically, the computational domain must be truncated without significant artifacts[15]. For a periodic structure analysis, where the periodic boundary condition is used, the computational domain is naturally truncated[11,13,15]. But sides of the computational domain, where PML is used, the computational domain can be truncated by PEC boundary condition given in eq. (6).

Periodic boundary conditions (PBCs)

Let's consider, an infinite periodic arrangement of 2D structures having period p along the x-direction (Figure 2). Hence, only E_y, H_x, H_z fields are present while other field component become zero. Because of the symmetry, only the fields in single unit cell are required to compute. Dashed lines represent boundaries of unit cell (in Figure 2). Solid black symbols denote fields that can be updated, whereas solid while symbols denote fields that cannot be updated. The PBCs can be used to compute field components that are not updated.

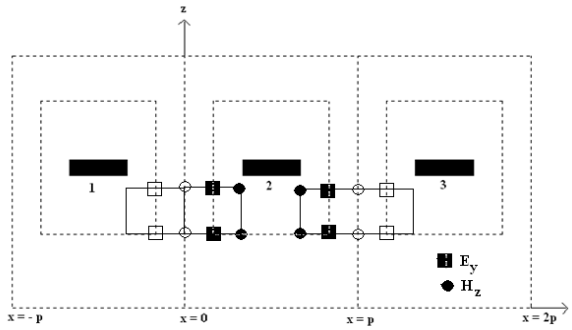

Figure 2: Infinite periodic structure with period '*p*' along the horizontal (*x*) direction.

The electromagnetic field for the PBCs can be with eq. (8)[28] and eq. (9)[28].

$$\underline{\boldsymbol{E}}(x=0,z) = \underline{\boldsymbol{E}}(x=p,z)e^{jk_xp}, \quad (8)$$

$$\underline{\boldsymbol{H}}(x=0,z) = \underline{\boldsymbol{H}}(x=p,z)e^{jk_xp}, \quad (9)$$

Where, k_x is propagation constant and p is the period of structure. k_x can be determined by $k_x = k_0.\sin\Theta = 2\pi f\sqrt{(\varepsilon_0\mu_0)}.\sin\Theta$[6,13].

In time domain, the fields become,

$$\underline{\boldsymbol{E}}(x=0,z,t) = \underline{\boldsymbol{E}}(x=p,z,t+p\sin\theta\,/c), \quad (10)$$

$$\underline{\boldsymbol{H}}(x=0,z,t) = \underline{\boldsymbol{H}}(x=p,z,t+p\sin\theta\,/c), \quad (11)$$

When a plane wave is incident perpendicular to periodic structure, k_x and θ would be zero. Consequently, the above equations (eq. (10)[28] and eq. (11)[28]) are reduced to following equations (eq. (12)[28] and eq. (13)[28]).

$$\underline{\boldsymbol{E}}(x=0,z,t) = \underline{\boldsymbol{E}}(x=p,z,t), \quad (12)$$

$$\underline{\boldsymbol{H}}(x=0,z,t) = \underline{\boldsymbol{H}}(x=p,z,t). \quad (13)$$

Above equations of PBCs can now be easily implemented in FDTD as follows (eq. (14) to (eq. (17)).

The magnetic field will satisfy

$$H_z^{(1,n_z,n_t)} = H_z^{(N_x-1,n_z,n_t)}, \quad (14)$$

and

$$H_z^{(2,n_z,n_t)} = H_z^{(N_x,n_z,n_t)}, \quad (15)$$

as well as the electric field will satisfy

$$E_y^{(1-1/2,n_z,n_t)} = E_y^{(N_x-1/2,n_z,n_t)}, \quad (16)$$

and

$$E_y^{(N_x+1/2,n_z,n_t)} = E_y^{(1+1/2,n_z,n_t)}. \quad (17)$$

IMPLEMENTATION

In order to implement PBC, consider FDTD model as shown in Figure 3, where a single unit cell surrounded by PBCs in horizontal directions (along *x*-direction) and absorbing boundary conditions (CPML) in vertical directions (along z-direction).

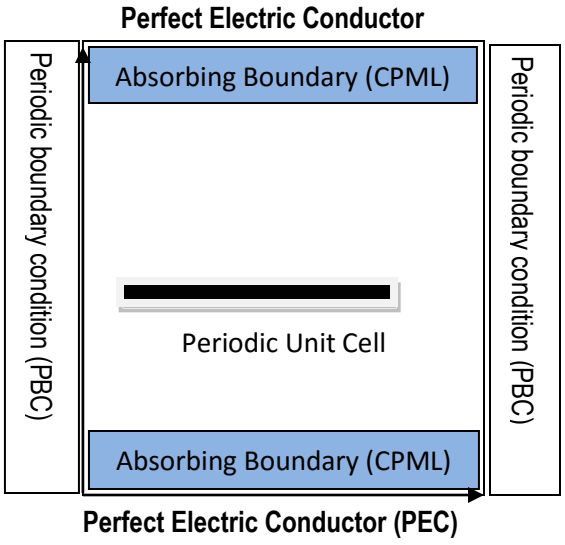

Figure 3: FDTD computational domain with PBC in *x*-(horizontal) direction and absorbing boundary condition (i.e. CPML) in z- (vertical) direction

The initial step is to build up the computational region together with geometry and sources, and all other parameters that will be required for FDTD computation. Field components are needed to be defined as arrays and initialized with zero values. At every time step, field components such as magnetic and electric fields are updated to time instant $(n+1)\Delta t$ and $(n+0.5)\Delta t$, respectively. In order to make computational domain as a finite space, a periodic boundary condition is enforced in horizontal direction and CPML in vertical direction. Therefore, field in boundaries is treated in accordance with specific boundary conditions during iteration. FDTD iterations are continued until some stopping criteria are achieved. Updated equations for FDTD (i.e. for TM_y case) can be determined by central difference formula as shown in Figure 1. In the interior domain, updated equations for 2-D TM_y case are implemented by using eq. (3) to eq. (5).

PBC is implemented in left and right side (in *x*-direction) of unit cell and absorbing boundary condition (CPML) along vertical direction as shown in Figure 3. Since periodic boundary condition is only employed in x-direction, therefore E_y and H_z components at boundaries are needed to be determined. For a normal incidence, implementation of PBC in FDTD is simple, because no data for future time is required. Field components of one side of the unit cell are related to other side as shown in Figure 2. Updating equations of PBCs for magnetic field and electric fields are implemented by utilizing eq. (14) to eq. (17).

RESULTS AND DISCUSSION

In this work, PBCs are implemented in FDTD. The PBC is applied at left and right side boundary of the computational domain (i.e. problem space). Absorbing boundary condition is employed at top and bottom of the computational domain. Size of computational domain is *260μm X 260μm*. Wavelength *(λ)* of the normalized source is set to be *λ=1.30μm*. Because the absorption spectra shows very low absorption in window from *λ=1.30μm - λ=1.55μm*. In order to demonstrate efficient implementation of PBCs, three different experiments are performed (i) vacuum filled computational domain, (ii) homogeneous periodic scatterers are placed at the computational domain, and (iii) inhomogeneous periodic slabs are placed.

Vacuum Filled Computational Domain

In first experiment, a point source is excited at the center of computational region filled with vacuum. The wavelength of source is $\lambda=1.30\mu m$. Figure 4 shows snapshots of E_y at different time steps in FDTD computational region, demonstrating the propagation of wave field. Figure 4(a) depicts initialization of the source at the center of computational domain. Source starts to march in time and space (see Figure 4(b)), as implemented in FDTD. Figure 4(c) depicts propagation of a point source over two-dimensional computational region. The effect of boundaries on the source is shown in Figure 4(d). When the source reaches near top and bottom boundaries of the computational domain, no wave is reflected from top and bottom boundaries (see Figure 4(d)). It is due to the implementation of the CPML absorbing boundary conditions with FDTD. All waves coming to top and bottom are absorbed by the CPML. Waves that reached at left and right side crossed along boundaries and propagated through left and right unit cells, respectively. No reflection is observed from left and right boundary (Figure 4(d)), due to the efficient implementation of PBCs. The waves seen in Figure 4(d) comes from other unit cells (i.e. left and right unit cells) depicting periodicity.

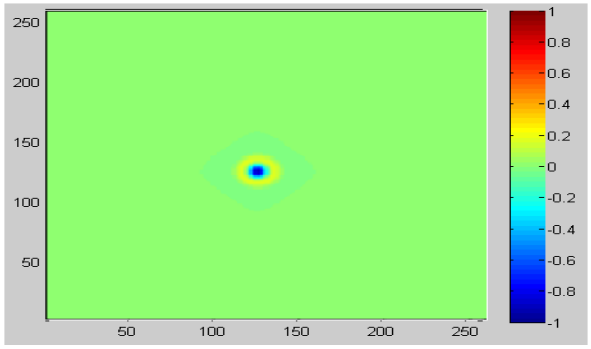

(a)

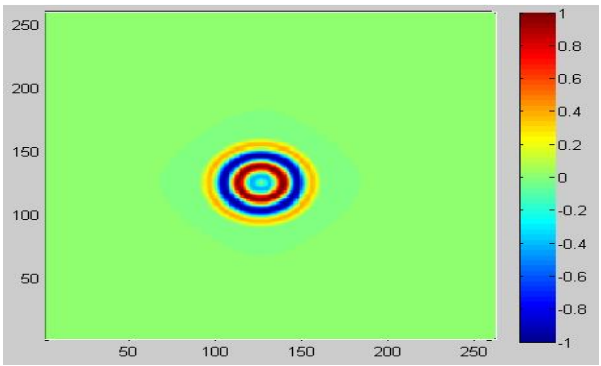

(b)

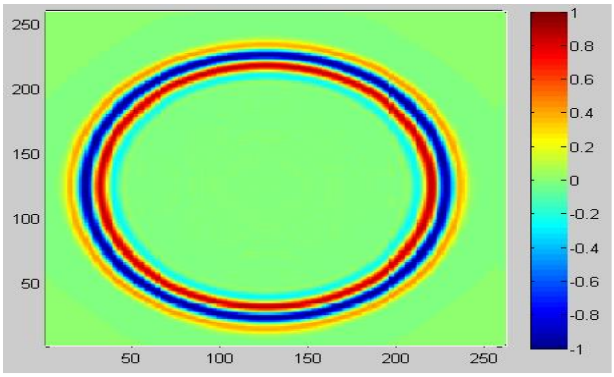

(c)

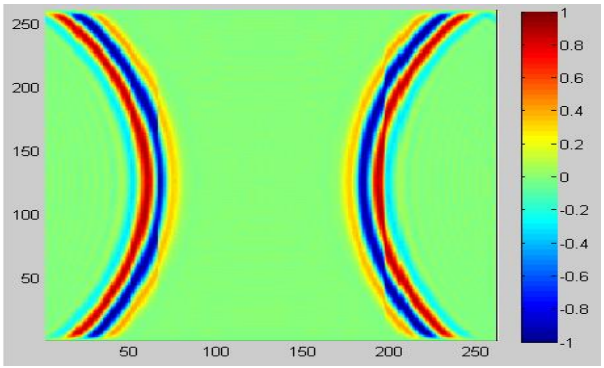

(d)

Figure 4: Propagation of electric field when a point source ($\lambda=1.30\mu m$) is excited at the center of problem space. Bottom horizontal and left vertical scale show size of the computational domain ($260\mu m$ X $260\mu m$). The right vertical scale show normalized amplitude of a point source. (a) initialization of source at center; (b)-(d) snapshots of field propagation for different time steps.

Effect of PBC in left boundary of computational domain is shown in Figure 5. Here, Figure 5(a) shows that the source is excited near left boundary of the computational domain. When the source is placed at left side, waves start to propagate and cross left boundary. Due to PBC at left side of the computational domain, waves crossing left boundary are observed in another cell which is in left of the chosen unit cell (i.e. computational domain). No reflection is observed from left boundary, as shown in Figure 5(b). The field that is shown (Figure 5(b)) to be near right boundary of computational domain is propagated from another cell which is beside the right boundary. This happened due to the PBC applied at right boundary. It is demonstrated that computational domain is a unit cell of an infinite periodic space. It means that there are infinite unit cells, and one unit cell for simulation is selected to save computational resources such as

memory and processing power. Therefore, sources that are excited at left boundary of each infinite unit cells are propagated through the boundary. Propagated field are then observed at right boundary of other unit cell which is besides that specific unit cell (see Figure 5(b)). Since, there is no reflection observed from boundary which demonstrates the efficient implementation of PBC at left boundary of computation domain.

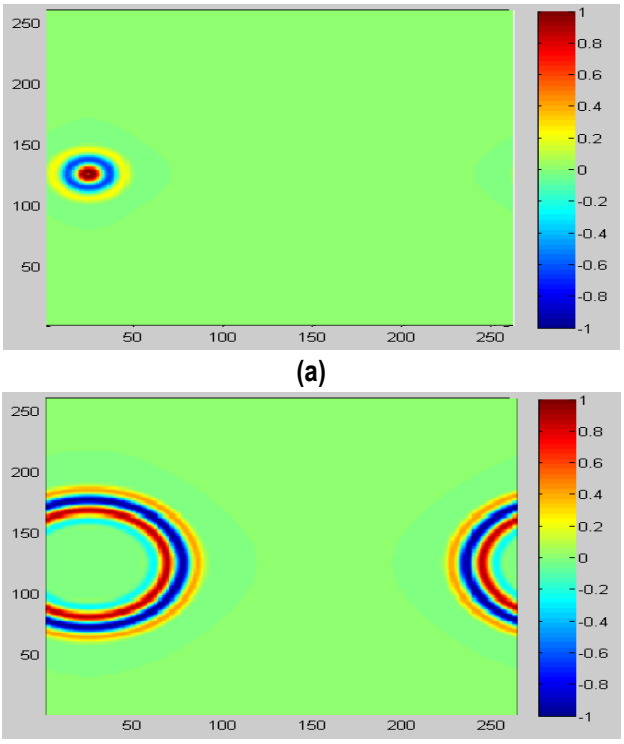

(a)

(b)

Figure 5: Snapshots of electric field propagation at different time steps, when a source is excited in the left side of the problem space. Bottom horizontal and left vertical scale show size of the computational domain (260*μm X* 260*μm*). The right vertical scale show normalized amplitude of a point source. (a) initialization of source at left side; (b) electric field crosses left boundary.

Similarly, effect of PBC applied at right boundary of computational domain is shown in Figure 6. Here, the source is excited near the right boundary of the computational domain as shown in Figure 6(a). When the source is placed at right side, waves start to propagate and cross right boundary. Due to PBC at right side of the computational domain, waves crossing right boundary would be observed in another cell which is in right of the chosen unit cell (i.e. computational domain). No reflection is observed from right boundary, as shown in Figure 6(b). The field that is shown (Figure 6(b)) to be near left boundary of computational domain is propagated from another cell which is beside the right boundary. This happened due to the PBC applied at right boundary, interpreting effect of infinite periodic structure. It is also observed that there is no reflection coming from right and left side of boundary. Since, there is no reflection observed from boundaries which demonstrates the efficient implementation of PBC at right and left boundary of computational domain.

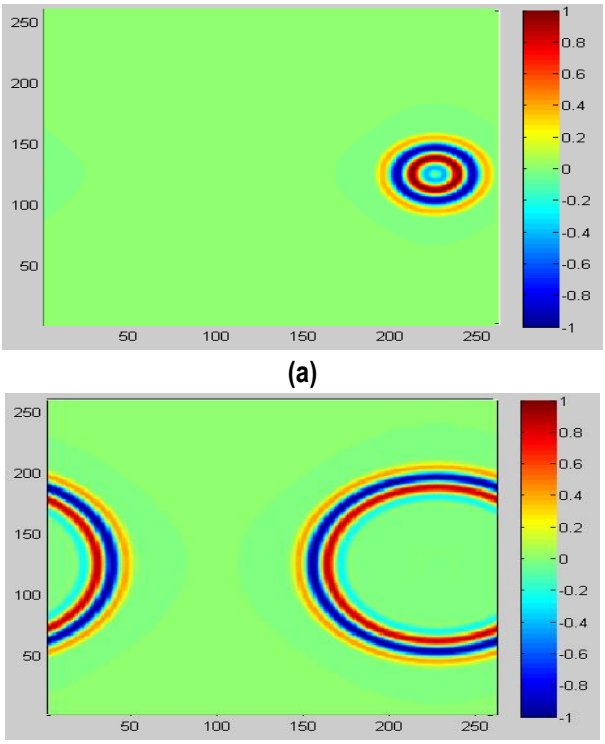

(a)

(b)

Figure 6: Snapshots of field propagation at different time steps, when a source is excited in right side of the problem space. Bottom horizontal and left vertical scale represents area of the computational domain (260*μm X* 260*μm*). Right vertical scale show normalized amplitude of a point source. (a) initialization of source at right side; (b) electric field crosses right boundary.

Homogeneous Periodic Material in Computational Domain

In second experiment, PEC scatterers are placed in computational domain with a periodicity of *a=13μm* in horizontal direction. Computational domain is filled with vacuum. PEC scatterers are positioned in the center of a vertical plane, as shown in Figure 7. Blue dashed lines are scatterers (see Figure 7). Length of each PEC

scatterer is ten times of the source wavelength (λ= *1.3μm)* i.e. *13μm*. A plane wave (i.e. line source) is excited above scatterers, as shown in Figure 7(a). After initialization of the plane wave, part of the wave propagates upward and part of the wave propagates downward, as shown in Figure 7(b). During the propagation of the wave, no reflection is observed from left and right boundary of computational domain. It is due to the efficient implementation of PBC on right and left boundary. Figure 7(c) shows upward propagating wave is absorbed by top boundary of the computational domain. It is demonstrated that there are no reflection coming from top boundary, due to implementation of the CPML absorbing boundary condition. The downward propagating wave hits the PEC scatterers (see Figure 7(c)). Since the PEC scatterers are placed periodically, the wave encounters the periodic scatterers would be diffracted, as shown in Figure 7(d). The diffraction phenomenon depends on the size of the scatterer related to source wavelength. As the length of the scatterer and size of slit is 10 times the source wavelength, therefore, all the wave encountering scatterer and slit get diffracted. The complete diffraction pattern is shown in Figure 7(d). Furthermore it is also observed that there are no reflections coming from left, right, and top and bottom boundaries of computational domain. This demonstrates efficient utilization of PBC and CPML boundary conditions.

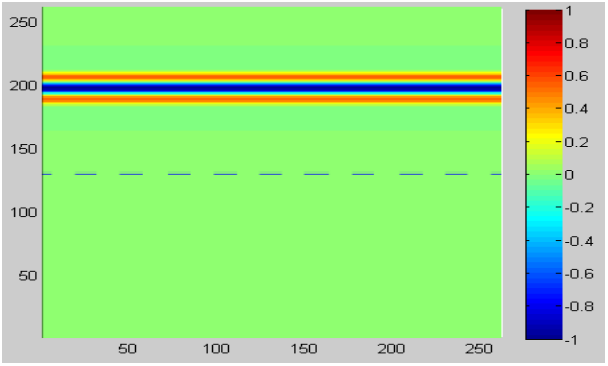

(a)

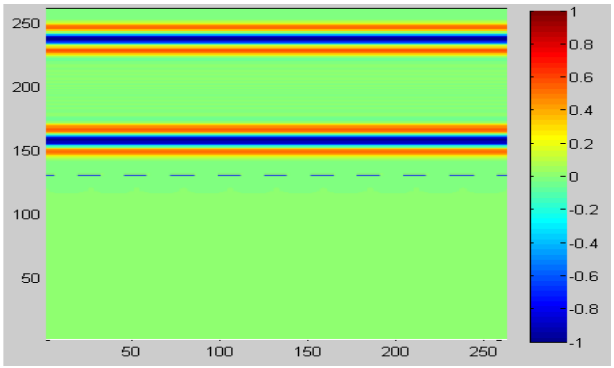

(b)

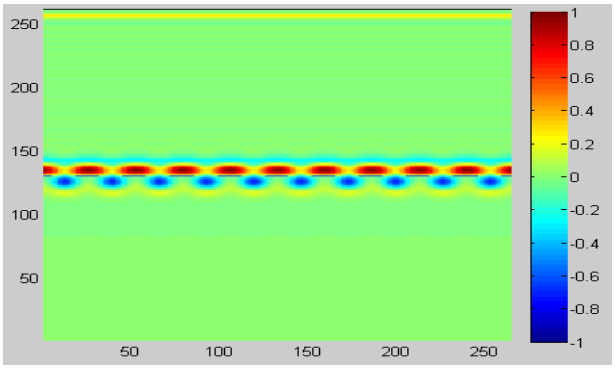

(c)

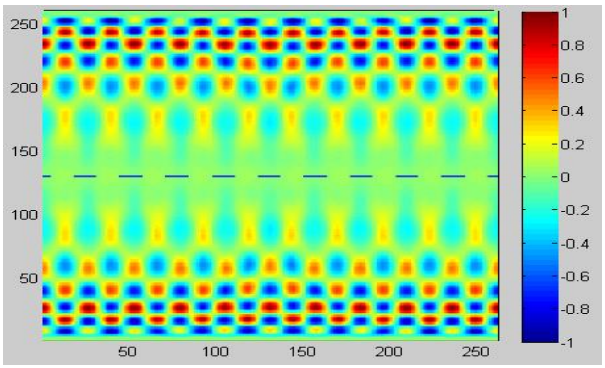

(d)

Figure 7: Snapshots of propagation of electric field at different time steps, when a plane wave is excited above the PEC periodic scatterers in *x*- (horizontal) direction of the problem space. Bottom horizontal and left vertical scale show size of the computational domain (260*μm X* 260*μm*). The right vertical scale show normalized amplitude of a point source. (a) initialization of line source at top of scatterer; (b) upward and downward propagating wave; (c) interaction of electric field with periodic PEC scatterer; (d) diffraction pattern of after interaction of wave and periodic PEC scatterer.

Inhomogeneous Periodic Material in Computational Domain

In third experiment, dielectric slabs are placed in

computational domain filled with vacuum, as shown in Figure 8. Thickness of slabs are $d = 13\mu m$, with a periodicity of $a=13\mu m$ in horizontal direction. Thickness of slab and periodicity are 10 times of the source wavelength ($\lambda = 1.30\mu m$). Slabs are placed at the center of vertical axis of computational domain, shown in Figure 8(a). Relative permittivity of a dielectric slab is $\varepsilon_r = 12$, and refractive index of a dielectric slab is computed by $n=\sqrt{\varepsilon_r} =\sqrt{12} = 3.46$. Here also a plane wave source is excited above periodic slabs to observe the interaction of plane wave with inhomogeneous periodic structures, as shown in Figure 8(a). After excitation, the wave is started to propagate in upward and downward direction in the computational domain, as shown in Figure 8(b). Two effects are demonstrated in Figure 8(c): (i) the absorption of upward propagating wave and (ii) the interaction of downward propagating wave to inhomogeneous periodic structure. The absorption of upward propagating layer in top boundary is due to the implementation of the absorbing layers boundary condition i.e. CPML in top and bottom boundaries. Since periodic slab and slit sizes are relative to source wavelength, the downward propagating wave after encountering with periodic structures get diffracted. One another phenomenon can also be observed in Figure 8(c) that the wave interacting with inhomogeneous slabs are not completely reflected from the surface of the slab. But the part of the wave is penetrated into slab and the other part of the wave is reflected from the surface of the slab. Since the slab has higher dielectric property as compared to vacuum filled computational domain, the velocity of the wave would be less inside the slab. The waves get resonating inside the slab, as shown in Figure 8(c). The diffraction pattern and resonance effect is shown in Figure 8(d). This illustrates the application of photonic crystal, as the photonic crystals have periodic structures.

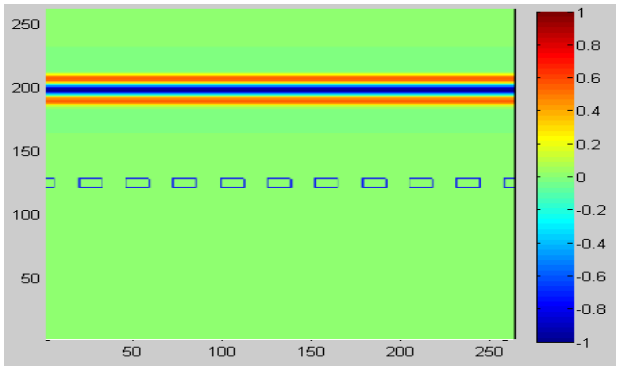

(a)

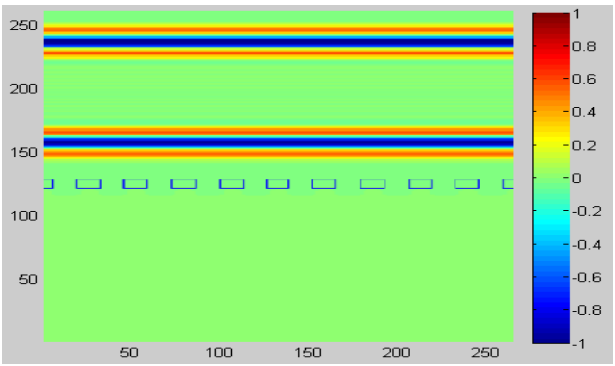

(b)

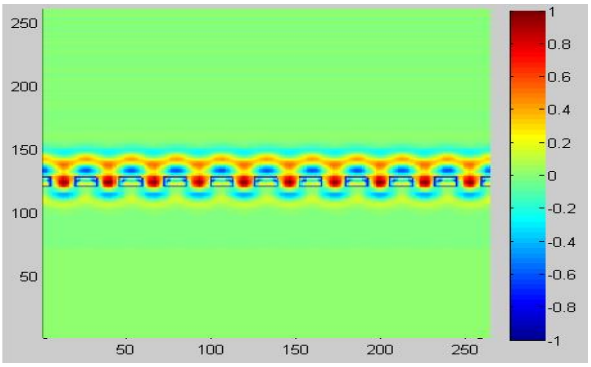

(c)

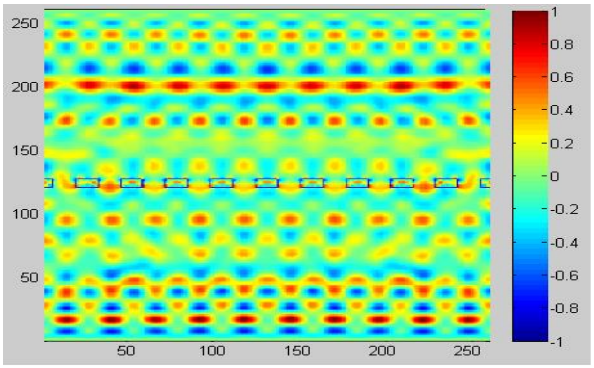

(d)

Figure 8: Snapshots of wave propagation at different time steps, when a plane wave is excited above the periodic dielectric slabs in *x*- direction (horizontal direction) of the problem space. Bottom horizontal and left vertical scale show size of the computational domain (260*μm X* 260*μm*). The right vertical scale show normalized amplitude of a point source. (a) initialization of line source at center; (b) upward and downward propagation of wave; (c) interaction of wave with periodic inhomogeneous dielectric slab; (d) diffraction and resonance pattern after wave interaction.

CONCLUSION

The PBCs have been implemented by using FDTD algorithm. The 2-dimensional computational domain is

described for the implementation of boundary conditions. The PBCs are implemented on the left and right side of the computational domain. The Floquet theory is used for the PBCs. Several simulation experiments have been performed to demonstrate the efficient working of PBCs. The experiments demonstrated that FDTD method can be employed in applications of periodic structures where periodicity is required. Some of the applications are photonic crystal, antenna arrays, and photonic filters.

REFERENCES

1. Yee KS. Numerical Solution of Initial Boundary Value Problems Involving Maxwell's Equations in Isotropic Media. IEEE Transaction on Antennas and Propagation. 1966; 14: 302-307.
2. Sumithra P, Thiripurasundari D. A Review on Computational Electromagnetics Method. Advanced Electromagnetics. 2017; 6 (1).
3. Han K, Chang C-H. Numerical Modeling of Sub-Wavelength Anti-Reflective Structures for Solar Module Applications. Nanomaterials. 2014; 4: 87-128.
4. Okada N, Cole JB. Effective Permittivity for FDTD Calculation of Plasmonic Materials. Micromachines. 2012; 3: 168-179.
5. Demir V. A Simple Implementation of FDTD-PBC Algorithm for Analysis of Periodic Structures. Journal of the Applied Computational Electromagnetics Society (ACES). 2014; 29 (12): 1018- 1024.
6. Yu J, Malekian R, Chang J, Su B. Modeling of Whole-Space Transient Electromagnetic Responses Based on FDTD and its Application in the Mining Industry. IEEE Transactions on Industrial Informatics. 2017; 13 (6): 2974-2982.
7. Yi Y, Chen B, Fang D-G, Zhou B-H. A New 2-D FDTD Method Applied to Scattering by Infinite Objects with Oblique Incidence. IEEE Transactions on Electromagnetics Compatibility. 2005; 47 (4): 756-762.
8. Lesina AC, Vaccari A, Berini P, Ramunno L. On the Convergence and Accuracy of the FDTD Method for nanoplasmonics. Optics Express. 2015; 23 (8): 10481-10497.
9. Jerez S, Lara, A. A High Resolution Nonstandard FDTD Method for the TM mode of Maxwell's Equations. Mathematical and Computer Modeling. 2011; 54 (7-8): 1852-1857.
10. Taflove A, Hagness SC. Computational Electrodynamics: The Finite-Difference Time-Domain Method. Artech House Publishing. 2000.
11. Rao N, Kumar VD. Investigation of a microstrip patch antenna with EBG structures using FDTD method. IEEE Recent Advances in Intelligent Computational Systems. 2011.
12. Zhang B, Hui XZ, Wu R, Qing SX. Analysis of Periodic Structures Using FDTD Method. Presented at Proceedings of the 9th International Symposium on Antennas, Propagation and EM Theory2010.
13. Chen J, Yang F, Qiang R. FDTD Method for Periodic Structures. Theory and Phenomena of Metamaterials. 2009.
14. Luebbers RJ, Hunsberger F. FDTD for Nth-Order Dispersive Media. IEEE Transaction on Antennas and Propagation. 1992; 40 (11).
15. Yang F, Samii YR. Electromagnetic Band Gap Structures in Antenna Engineering. Cambridge University Press. 2009.
16. Tsay W, Pozar DM. Application of the FDTD Technique to Periodic Problems in Scattering and Radiation. IEEE Microwave and Guided Wave Letters. 1993; 3 (8).
17. Hu S, Gao T, Li H, Yang B, Jiang Z, Liu L, Chen M. Application of Convolution Perfectly Matched Layer in MRTD Scattering Model for Non-Spherical Aerosol Particles and its Performance Analysis. Journal of Quantitative Spectroscopy and Radiative Transfer. 2017; 200: 1-11.
18. Elsherbeni A, Demir V. The Finite-Difference Time-Domain Methods for Electromagnetics with MATLAB Simulations. Scitech Publishing. 2009.
19. Uslu A, Apaydin G, Sevgi L. Diffraction Modeling by a Soft--Hard Strip Using Finite-Difference Time-Domain Method. IEEE Antennas and Wireless Propagation Letters. 2016: 16: 306-309.
20. Diener JE, Quimby J, Remley KA, Elsherbeni AZ. Millimeter-wave frequency FDTD simulation for error vector magnitude of modulated signals. Paper presented at International Applied Computational Electromagnetics Society Symposium (ACES)2018.
21. Dong M, Chen J, Zhang A. A Convolutional Perfectly Matched Layer (CPML) for the Fourth-Order One-Step Leapfrog HIE-FDTD Method. Applied Computational Electromagnetics Society Journal. 2018; 33 (1): 1-6.
22. Roden JA, Gedney, SD. Convolution PML(CPML): An Efficient FDTD Implementation of the CFS-PML for Arbitrary Media. Microwave and Optical Technology Letters. 2000; 27(5).
23. Gvozdic BD, Djurdjevic DZ. Performance advantages of CPML over UPML absorbing boundary conditions in FDTD algorithm. Journal of Electrical Engineering. 2017; 68 (1): 47-53.
24. Dong Y, Zhou J. Absorbing boundary conditions in leapfrog ADI-FDTD method. Paper presented at Progress in Electromagnetics Research Symposium-Fall (PIERS-Fall)2017.
25. Jiang HL, Zhang JF, Jiang WX, Cui TJ. Unconditionally Stable CN-PML Algorithm for Frequency-Dispersive Left-Handed Materials. IEEE Antennas and Wireless Propagation Letters. 2017; 16: 2006-2009.
26. He G-Q, Stiens JH, Shao W, Wang B-Z. Recursively Convolutional CFS-PML in 3-D Laguerre-FDTD Scheme for Arbitrary Media. IEEE Transactions on Microwave Theory and Techniques. 2018; 66 (5): 2070-2079.
27. Okano M, Noda S. Analysis of multimode point-defect cavities in three-dimensional photonic crystals using group theory in frequency and time domains. Phys. Rev. B. 2004; 70 (12): 125105.
28. Carmona R, Delarue F. Probabilistic Theory of Mean Field Games with Applications I. Springer Cham. 2018; 83: 713.